Effects of Effusion Cooling Pattern Near the Dilution Hole for a Double-Walled Combustor Liner—Part II: Flowfield Measurements

Adam C. Shrager[1]
Mem. ASME
Department of Mechanical and Nuclear Engineering,
The Pennsylvania State University,
127 Reber Building,
University Park, PA 16802
e-mail: adam.shrager@gmail.com

Karen A. Thole
Mem. ASME
Department of Mechanical and Nuclear Engineering,
The Pennsylvania State University,
136 Reber Building,
University Park, PA 16802
e-mail: kthole@psu.edu

Dominic Mongillo
Pratt & Whitney,
400 Main Street,
East Hartford, CT 06118
e-mail: dominic.mongillo@pw.utc.com

The complex flowfield inside a gas turbine combustor creates a difficult challenge in cooling the combustor walls. Many modern combustors are designed with a double-wall that contain both impingement cooling on the backside of the wall and effusion cooling on the external side of the wall. Complicating matters is the fact that these double-walls also contain large dilution holes whereby the cooling film from the effusion holes is interrupted by the high-momentum dilution jets. Given the importance of cooling the entire panel, including the metal surrounding the dilution holes, the focus of this paper is understanding the flow in the region near the dilution holes. Near-wall flowfield measurements are presented for three different effusion cooling hole patterns near the dilution hole. The effusion cooling hole patterns were varied in the region near the dilution hole and include: no effusion holes; effusion holes pointed radially outward from the dilution hole; and effusion holes pointed radially inward toward the dilution hole. Particle image velocimetry (PIV) was used to capture the time-averaged flowfield at approaching freestream turbulence intensities of 0.5% and 13%. Results showed evidence of downward motion at the leading edge of the dilution hole for all three effusion hole patterns. In comparing the three geometries, the outward effusion holes showed significantly higher velocities toward the leading edge of the dilution jet relative to the other two geometries. Although the flowfield generated by the dilution jet dominated the flow downstream, each cooling hole pattern interacted with the flowfield uniquely. Approaching freestream turbulence did not have a significant effect on the flowfield. [DOI: 10.1115/1.4041153]

Introduction

Given the high temperatures in a modern gas turbine combustor, cooling the walls of the combustion chamber is critical for durability. Modern gas turbine engines commonly use double-walled combustor liners that contain both impingement and effusion cooling plates. The purpose of the impingement cooling is to enhance the backside internal cooling, while the effusion cooling protects the external walls by creating a protective film of coolant on the surface. Modern combustors also require the use of large dilution jets for mixing the fuel and air as well as generating high levels of turbulence. The mixing provided by the dilution jets allows for lean burning, which reduces NO_x emissions.

Cooling the liner walls is particularly difficult near the dilution holes due to the complex interactions of the effusion flow with the high-momentum dilution jets. In order to better understand the flow near the dilution hole, the current study evaluates the flowfield for a double-walled combustor liner with three effusion cooling patterns that were varied near the dilution holes. The effusion hole patterns include: no surrounding effusion cooling (closed); a ring of effusion holes blowing radially outward from the dilution hole (outward); and a ring of effusion holes blowing radially inward into the dilution hole (inward). Flowfield measurements were made in the centerline plane for each of the effusion hole patterns.

The objective of this paper is to evaluate the flow in the region surrounding the dilution hole. The flowfield of each effusion pattern will also be evaluated over a range of momentum flux ratios and at two different approaching freestream turbulence intensities. The results provide a unique understanding of how different effusion cooling patterns interact with the dilution jet for a realistic combustor geometry. In addition, this paper will also provide a brief discussion on how the flowfields relate to the surface cooling measurements, which were presented in a companion paper [1].

Relevant Past Studies

There have been several past studies that have documented the complex three-dimensional flowfield of a jet in crossflow. There have also been multiple studies that evaluated the flowfields of combustor relevant geometries with dilution jets interacting with a coolant layer produced from either discrete effusion holes or a slot. This section reviews the fundamental flowfield of a jet in crossflow alone, the fundamental flowfield of effusion cooling without dilution jets, and the combined flowfield effects of a dilution jet interacting with either effusion or slot cooling. All relevant studies with effusion cooling contained angled holes and were for single-walled combustor liners.

Through extensive flow visualization of a jet in crossflow, Fric and Roshko [2] showed that there were multiple vortical structures that formed from the interactions of the jet and freestream. A horseshoe vortex formed at the leading edge of the jet, shear layer vortices rolled up the sides of the jet, a pair of counter-rotating vortices developed as the jet was bent over with the freestream flow, and wake vortices formed behind the jet. In addition, Fric and Roshko observed that at low velocity ratios, the jet remained closer to the surface, even entraining some of the near-wall flow.

Kelso et al. [3] also used flow visualization to evaluate a jet in crossflow and found the same vortical flow structures as Fric and Roshko [2]. In addition, Kelso et al. showed that flow from the

[1]Corresponding author.

Manuscript received July 8, 2018; final manuscript received July 23, 2018; published online October 15, 2018. Editor: Jerzy T. Sawicki.

freestream was drawn toward the leading edge of the jet. Just above the leading edge of the jet hole, the flow was either drawn into the jet hole or formed a horseshoe vortex just upstream. They also found that the flow at the leading edge of the jet was very unsteady as a result of the vortices. Multiple other jets in crossflow studies have also found evidence of downward motion of the freestream into a jet hole [4–6]. Andreopoulos [4] found that there was an adverse pressure gradient inside the leading edge of the jet hole. At low velocity ratios, the boundary layer inside the jet hole separated and created a recirculation region that drew fluid from the freestream. Peterson and Plesniak [5] measured the flowfield inside the jet hole and found a region of reversed flow and separation at the leading edge, which was thought to be caused by ingestion of freestream fluid into the hole. Additionally, in an unsteady computational study, Holloway and Walters [6] found ingestion of freestream flow into the leading edge of the jet hole due to low pressure inside the hole.

Kelso et al. [3] also measured time-averaged velocity fields for a jet in crossflow and found that behind the jet, there was a stagnation point that dictated where the flow was either entrained into the jet or convected downstream. In a numerical jet in crossflow study, Sykes et al. [7] also observed a stagnation point behind the jet. In addition, Scrittore [8] found a similar downstream stagnation point to these jet in crossflow studies for a single-walled combustor liner with effusion cooling and dilution jets.

Holdeman and Walker [9] evaluated multiple arrangements of dilution jets without effusion holes at momentum flux ratios ranging from $I_D = 6$–60. These researchers found that the momentum flux ratio was the most important flow parameter that affected the jet penetration and the mixing. They also found that for a given dilution hole diameter, increasing the spanwise spacing of the dilution holes resulted in nonuniform, three-dimensional flow effects.

For a single-walled effusion liner without dilution jets, Scrittore et al. [10] found that the velocity profiles and turbulence levels of the effusion jets scaled with the blowing ratio of the effusion jets. In addition, they found that once the flow was fully developed, the momentum flux ratio of the effusion jets did not affect the penetration height. In another flow visualization study of an effusion liner without dilution holes, Fric et al. [11] found that the film coverage from the effusion jets was made worse as the blowing ratio increased between $M_{\text{eff,in}} = 1.7$–3.3, while the coverage of the effusion film improved beyond this range, resulting from an increased level of coolant.

Scrittore [8] evaluated a single-walled combustor liner that contained a row of dilution holes with and without effusion cooling to measure the impact of the effusion flow on the flowfield created by the dilution jets. Through this study, Scrittore found that the dilution jet flowfield was sensitive to the effusion flow. Even though the penetration height of the effusion jets was minimal, the added upward momentum from the effusion jets resulted in less negative vertical velocities as high as the midspan of the test section, compared to the case without effusion cooling. Additionally, without effusion cooling, a vortex formed along the lateral edge of the dilution jet, which resulted in a localized region of high streamwise velocity at the lateral edge of the dilution jet. However, when effusion cooling was added, the vorticity was significantly reduced and the region of high streamwise velocity shifted higher off the surface.

For a different single-walled combustor liner with effusion cooling and dilution holes, Vakil and Thole [12] found a large recirculation region downstream of the dilution jet that transported warm flow toward the surface. This recirculation was propagated by the counter-rotating vortices that were developed by the dilution jet. They also found that a significant amount of the coolant downstream of the dilution jet was lifted off the surface due to entrainment into the dilution jet, resulting in a thin coolant layer. This lift-off of coolant downstream of the dilution jet was also observed by Martiny et al. [13] for a slot film interacting with a dilution jet and by Scrittore et al. [14] for a single-walled combustor liner with effusion cooling and dilution jets, similar to the geometry presented by Vakil and Thole. Additionally, Scrittore et al. found that for the same dilution jet flow, a higher momentum flux ratio for the effusion jets ($I_{\text{eff,in}} = 25$) resulted in a thicker coolant layer behind the jet compared to a lower momentum flux ratio ($I_{\text{eff,in}} = 12$) due to the presence of more effusion cooling flow.

Given the limited information about the flowfield near the dilution hole with effusion cooling in the previous literature, the current study is unique in that it presents detailed flow measurements that are focused in the region near the dilution hole. In addition, this study presents multiple effusion hole patterns, varied near the dilution hole, that provide insight into how different effusion jet orientations affect the flow upstream and downstream of the dilution jet. The current study also uses a realistic double-walled combustor liner geometry.

Experimental Methods

Flowfield measurements of a combustor liner were made in in a low speed, closed-loop wind tunnel. The combustor simulator used in this study is the same as described in a companion paper [1] and is a modification of the combustor simulator previously described by Vakil and Thole [12] and Scrittore et al. [14]. The flow is driven by an axial fan and sent through a mainstream and secondary path. The mainstream flow is sent through conditioning screens before entering the test section, shown in Fig. 1. In the test section, the area reduces at a contraction ratio of 1.8:1 with symmetric quarter rounds, located at $x/D = -36.5$, where D is the diameter of the dilution hole and the origin is at the center of the dilution hole. The height of the test section was 0.55 m with a width of 1.11 m.

A turbulence grid, shown in Fig. 1, which is modeled after a grid used by Schroeder and Thole [15], is used to achieve high approaching freestream turbulence intensity of $\text{Tu} = 13\%$ at the first row of effusion holes located at $x/D = -2$. The grid is composed of large vertical bars of diameter, $b = 42$ mm, each spaced apart $2b$ center-to-center. The turbulence grid is located at $x/D = -16.2$, which is 10 bar diameters ($10b$) upstream of the first row of effusion holes. Without the turbulence grid, the approaching freestream turbulence intensity is $\text{Tu} = 0.5\%$.

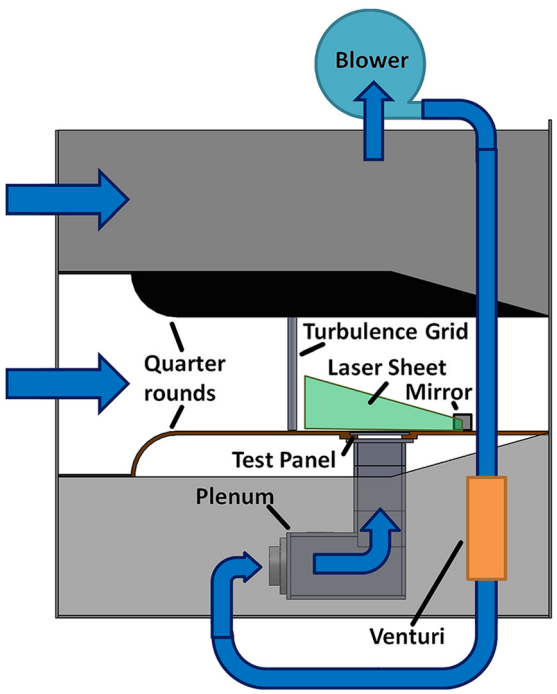

Fig. 1 Illustration of the combustor simulator test

The mainstream velocity was measured with a pitot-static probe, set 0.2 m upstream of the turbulence grid in the midheight and midspan of the wind tunnel. The mainstream velocity was maintained at 3.4 m/s for each of the test cases presented. Although the mainstream was not heated, the mainstream temperature was measured as an average of six thermocouples that were evenly spaced across the midspan of the wind tunnel, which indicated a uniform temperature field to within 1 °C.

Also shown in Fig. 1 is the coolant loop, which supplied the effusion and dilution jet flow. The flow through the secondary path is driven by a blower that was installed on the top section of the wind tunnel. The coolant flowrate is measured with a venturi flow meter before the flow enters a supply plenum and exits through the double-walled combustor liner. The supply plenum contained six evenly spaced thermocouples to measure the coolant temperature, which indicated a uniform temperature field to within 0.2 °C. Flow tests were performed at a density ratio of 1.

The test panel presented in this paper was a double-walled combustor liner with both impingement and effusion cooling plates, shown in Fig. 2. Note that Fig. 2 highlights the measurement plane along the centerline of the dilution hole and only shows 33% of the span. Also, note that the measurement plane contains effusion holes, which were located in rows 5 and 15. The geometry was repeated so that there were 15 dilution holes to span the entire width of the wind tunnel and to ensure periodicity. The same panel geometry was presented in a companion paper [1] and was originally modeled after a single-walled effusion liner with dilution holes presented by Scrittore [8]. Flow from the supply plenum traveled through the impingement holes, which then fed the effusion holes. The dilution holes, which had a diameter of $D = 29.6$ mm, were directly fed from the supply plenum. The pitchwise spacing of each dilution hole was $2.1D$ and the radially surrounding effusion holes were located $0.69D$ from the center point of each dilution hole. The geometry and parameters of the effusion and impingement holes are defined in Fig. 3. Note that the spacing of the impingement holes, indicated by dashed lines, was the same as the spacing for the effusion holes, indicated by solid lines; however, the impingement holes were staggered a distance of $1.8d$ from the effusion holes, where d is the diameter of the effusion and impingement holes. Also note that there were no impingement holes in the region near the dilution hole to isolate the effects of the different effusion cooling patterns.

As was previously mentioned, the purpose of this study was to evaluate the flowfields of different effusion cooling patterns surrounding the dilution hole. The closed pattern, without any surrounding effusion holes, is shown in Fig. 4(*a*). The outward and inward patterns, shown in Figs. 4(*b*) and 4(*c*), respectively, included additional effusion holes that radially surrounded the dilution hole and were pointed either outward or inward toward

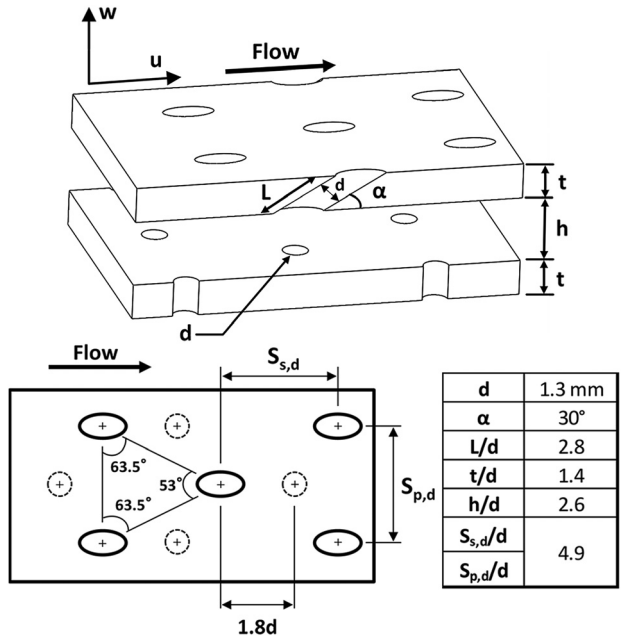

d	1.3 mm
α	30°
L/d	2.8
t/d	1.4
h/d	2.6
$S_{s,d}/d$	4.9
$S_{p,d}/d$	

Fig. 3 Illustration of the effusion and impingement holes detailing the geometry and parameters as well as defining *u* and *w* velocity directions. Note for the top down view, solid lines indicate effusion holes and dashed lines indicate impingement holes.

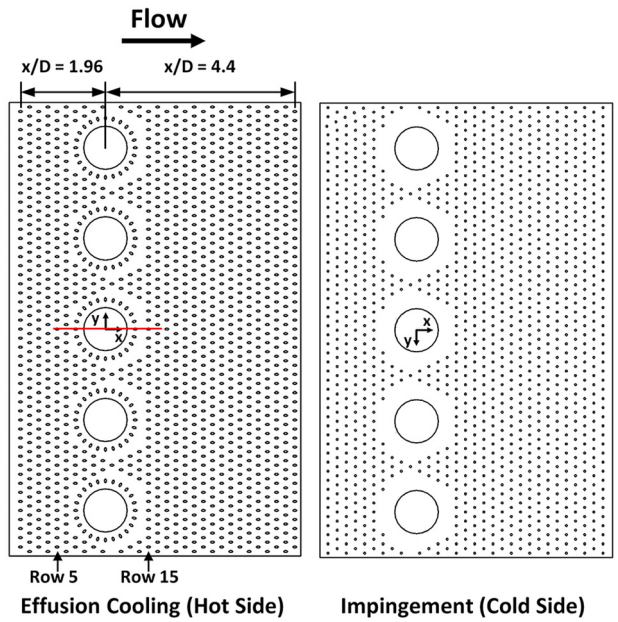

Fig. 2 Illustration of the center portion (33% of the span) of the combustor panel including the effusion and impingement plates with a pitchwise spacing of the dilution holes at $2.1D$. The flowfield measurement plane is defined by the line along the central dilution hole and contains effusion holes in rows 5 and 15.

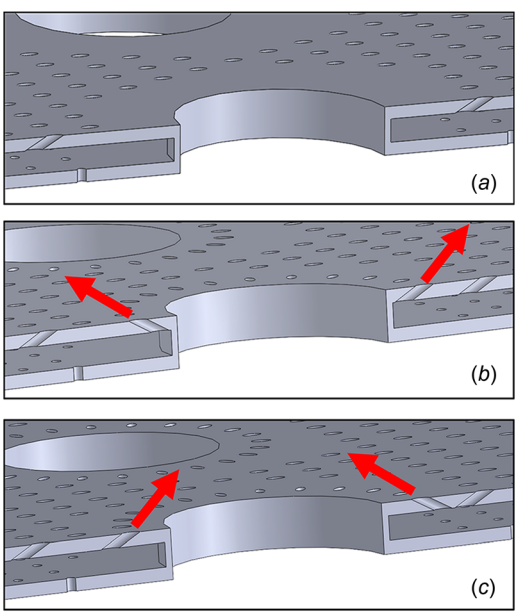

Fig. 4 Cross-sectional view of the cooling patterns near the dilution hole for the (*a*) closed, (*b*) outward, and (*c*) inward cases

the dilution hole, respectively. The test panels used in this study were additively manufactured from glass-filled nylon with powder bed fusion. The closed pattern was made by filling the radially surrounding effusion holes with water soluble wax.

Each of the three effusion cooling patterns was evaluated over a range of dilution jet momentum flux ratios, including $I_D = 30$, 20, and 11. Because the effusion and dilution holes were supplied by the same plenum, the percentage of mass flow through each set of holes was experimentally determined. The pressure difference across the panel was measured with static pressure taps that were installed inside the supply plenum and on the external surface of the panels. Over a range of pressure ratios, flow parameters were evaluated for the panels with and without the dilution holes plugged. At a given pressure ratio, the difference in the flow parameter curves represented the amount of flow through just the dilution holes. For the $I_D = 30$ case, 73% of the coolant supply flow went through the dilution holes and the other 27% went through the effusion holes. For the other two dilution jet momentum flux ratios, 74% and 75% of the supply flow went through the dilution holes for the $I_D = 20$ and 11 cases, respectively. In addition, the inlet momentum flux ratio based on the effusion jets, $I_{eff,in}$, and the dilution jet and effusion jet blowing ratios, M_D and $M_{eff,in}$, were determined for each of the cases. Table 1 summarizes the test conditions, which were based off of the inlet velocity at the start of the test panel. The characteristic length, l, that defines the inlet Reynolds number, Re_{in}, spans from the quarter round at $x/D = -32.3$ to the inlet at $x/D = -2$.

Due to the addition of mass through the effusion and dilution holes, there was a local increase of the mass-averaged freestream velocity, which decreased the local momentum flux ratio of the effusion jets. Figure 5 shows the reduction of the local momentum flux ratio for the effusion jets, I_{eff}, normalized by the inlet momentum flux ratio of the effusion jets, $I_{eff,in}$. The local mass-averaged velocity was calculated with the inlet velocity and the added mass at each row of effusion holes. The $I_{eff,in} = 24$ case had the largest reduction of local momentum flux ratio at 11.7% because more coolant was added into the flow compared to the other two cases. The local momentum flux ratio reductions of the $I_{eff,in} = 15$ and 7 cases were 9.7% and 7.2%, respectively. Due to the large test section and minimal change in the pressure ratio across the panel, the additional mass added to the flow did not have a large impact on the local momentum flux ratio.

Flowfield Measurement Methods. Flowfields were measured near the central dilution hole along the centerline plane, shown in Fig. 1, using two-dimensional particle image velocimetry (PIV). Using a dual-head laser, seed particles were illuminated and tracked with a high-speed camera. The seed particles were atomized with an aerosol generator and fed into the wind tunnel. The laser sheet entered normal to the freestream through a glass window. As shown in Fig. 1, the beam was turned 90 deg by a mirror that was placed far downstream of the test panel so it would not affect the flow. The camera was placed normal to the laser plane. Given the placement of the camera, the images had a resolution of 11 pixels/mm. 4000 sets of image pairs captured at 1000 Hz were averaged together to generate time-averaged flowfields, which was sufficient to achieve statistical convergence. The time delay between each image pair was 30 μs, which resulted in near-wall particle displacement of 6–8 pixels. The particle displacements in the dilution jet flow were typically 14 pixels, given the higher velocities. Velocities were calculated using a multipass scheme

Table 1 Summary of test cases

Tu (%)	I_D	$I_{eff,in}$	M_D	$M_{eff,in}$	DR	Re_{in}
0.5	30	24	5.7	5.1	1.08	1.9×10^5
13	30	24	5.7	5.1	1.08	1.9×10^5
13	20	15	4.7	4.0	1.08	1.9×10^5

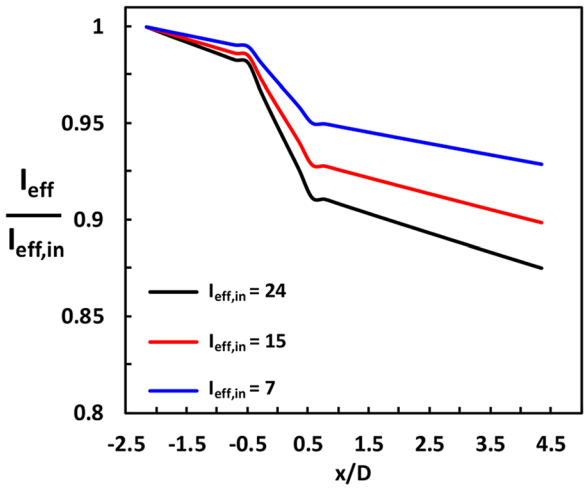

Fig. 5 Local effusion momentum flux ratio, I_{eff}, normalized by inlet effusion momentum flux ratio, $I_{eff,in}$, for each of the flow conditions

with decreasing interrogation windows, finishing with a window size of 16×16 pixels and 50% overlap. The images were processed using commercial software [16].

Uncertainty Analysis. An uncertainty analysis was performed for the variables describing the test conditions and the overall effectiveness measurements. Bias uncertainties were determined using the partial differentiation method presented by Moffat [17]. The bias uncertainty calculated for I_D was at most $\pm 12\%$ for $I_D = 11$ and $\pm 11\%$ for $I_D = 30$. The bias uncertainty for $I_{eff,in}$ was at most $\pm 17\%$ for $I_{eff,in} = 7$ and $\pm 15\%$ for $I_{eff,in} = 20$. The precision uncertainties, as described by Figliola and Beasley [18] for a 95% confidence interval, of the momentum flux ratio measurements were determined to be negligible.

Repeatability tests were also performed to determine precision uncertainty of the PIV measurements for a 95% confidence interval [18]. The same case was repeated four separate times on multiple days. Upstream of the dilution jet, precision uncertainty near the wall was found to be $\pm 3\%$ for u, $\pm 2\%$ for w, and $\pm 3\%$ for TL. Downstream of the dilution jet, precision uncertainty near the wall was found to be $\pm 9\%$ for u, $\pm 3\%$ for w, and $\pm 5\%$ for TL.

Flowfield Results

Flowfield measurements were made along the centerline plane of the central dilution hole for the closed, outward, and inward effusion hole patterns. First, the effects of the different effusion hole patterns will be discussed for the flowfields near the dilution hole at an approaching high freestream turbulence of Tu = 13%. Next, the impact of momentum flux ratio on the flowfield for each geometry will be evaluated. Finally, the effects of approaching freestream turbulence intensity will be discussed with a comparison to low approaching freestream turbulence, Tu = 0.5%.

Effects of the Effusion Hole Pattern. To observe the effects of the different effusion hole patterns near the dilution hole, flowfields were evaluated for the closed, outward, and inward geometries. Figures 6(*a*)–6(*c*) show contours of turbulence level with time-averaged streamlines in the centerline plane for the baseline flow conditions of $I_D = 30$ and Tu = 13%. Note that the turbulence levels reported are the root-mean-square of the two fluctuating velocity components normalized by the incoming freestream velocity. In all three configurations, the dilution jet streamlines and turbulence levels were nearly identical, indicating that the effusion cooling configurations had little effect on the core of the dilution jet above the wall. Turbulence levels downstream of

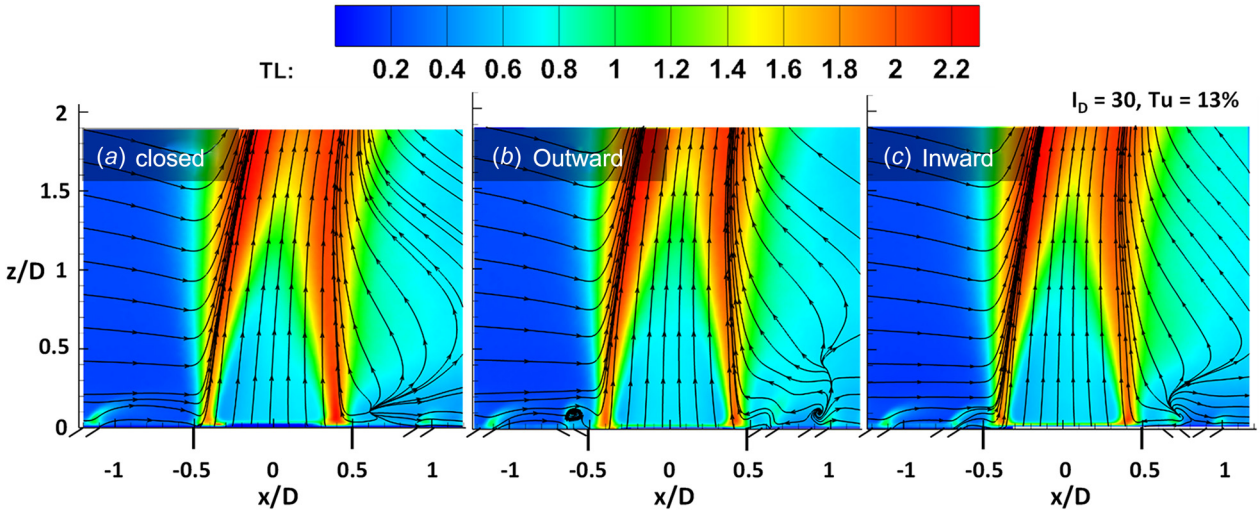

Fig. 6 Contours of the turbulence levels and time-averaged streamlines in the centerline plane for the (*a*) closed, (*b*) outward, and (*c*) inward geometries at $I_D = 30$ and Tu = 13%

the dilution jet were significantly higher than upstream due to the shear and unsteady dilution jet. Also shown in Figs. 6(*a*)–6(*c*) are effusion jets at $x/D = -1.1$ and 0.9 for all cases that correspond with effusion cooling rows 5 and 15, respectively, as labeled in Fig. 1. Because the upstream geometries were the same, the row 5 effusion jet was similar for each case, with jet lift-off and high turbulence levels resulting from the shear, as shown in Figs. 6(*a*)–6(*c*). Between $x/D = -0.75$ and 0.75, the near-wall flowfield for each case differed. In this region, the outward and inward cases contained additional effusion holes surrounding the dilution hole, as compared to the closed case.

Of the three effusion cooling patterns, the outward case (Fig. 6(*b*)) resulted in a significantly different flowfield compared to the closed and inward cases (Figs. 6(*a*) and 6(*c*)), generating vortices upstream and downstream of the dilution hole. Figure 6(*b*) shows that for the outward case, the shear between the effusion jet and freestream resulted in a clockwise vortex at the leading edge of the dilution hole. Similar to a horseshoe vortex, this vortex transported freestream flow toward the surface. For the inward case, shown in Fig. 6(*c*), the effusion jet just upstream of the dilution hole, had a similar shape and magnitude relative to the row 5 jet. Compared to the closed case, the inward blowing effusion jet did not significantly alter the flow near the leading edge of the dilution hole since the coolant was directly injected into the dilution jet.

Downstream of the dilution hole, there were notable differences in the flowfields resulting from effusion hole patterns as shown in Figs. 6(*a*)–6(*c*). The closed and inward geometries (Figs. 6(*a*) and 6(*c*)) were similar with stagnation regions in the flowfield just downstream of the dilution jet. The stagnation region defined the location where the flow was either entrained into the dilution jet or was convected downstream. Kelso et al. [3] and Sykes et al. [7] documented a similar stagnation region behind a jet in crossflow. Similarly, Scrittore [8] found a stagnation region downstream of the dilution jet for a single-walled combustor liner with effusion cooling and dilution jets. There were also differences between the closed and inward cases downstream of the dilution hole. Compared to the closed case, the additional effusion jet for the inward case caused the stagnation region to shift slightly downstream with a weak vortex that formed at the trailing edge of the dilution hole.

In contrast to the closed and inward cases, the outward case (Fig. 6(*b*)) was significantly different. Just downstream of the dilution hole, the outward blowing effusion jet was injected nearly vertically and then entrained into the dilution jet. Because of the trajectory of the outward effusion jet, the stagnation region shifted downstream just above the leading edge of the row 15 effusion hole ($x/D = 0.9$). At the stagnation region, the shear between the entrained flow and the row 15 effusion jet resulted in a counterclockwise vortex that caused considerable jet lift-off of the row 15 effusion jet.

Figures 7(*a*)–7(*c*) show close up turbulence level contours with velocity vectors at the leading edge of the dilution hole for each geometry at $I_D = 30$ and Tu = 13%. Upstream of the dilution hole, Figs. 7(*b*) and 7(*c*) show high levels of turbulence due to the shear of the outward and inward effusion jets, respectively. For all three geometries, there was significant downward motion of the flow toward the leading edge of the dilution hole that could lead to ingestion into the dilution hole. The downward motion shown in Figs. 7(*a*)–7(*c*) was consistent with previous literature for a jet in crossflow. As shown by Kelso et al. [3], from the freestream was ingested into the leading edge of the jet hole. In addition, Andreopoulos [4] and Peterson and Plesniak [5] found a region of flow separation occurred inside the jet hole at the leading edge. A similar region of flow separation was also found in a computational study by Holloway and Walters [6], which resulted in a low pressure region that drew flow from the freestream into the jet hole at the leading edge. Additionally, in a single-walled combustor liner study with effusion cooling and dilution jets, Scrittore [8] showed flowfield measurements with downward trajectories toward the leading edge of the dilution hole that were similar to the current study.

Figure 7(*a*) shows that there was a significant amount of downward motion at the leading edge of the dilution hole for the closed case, which was due to the previously mentioned low pressure region inside the dilution hole. In comparison to the closed case, the vortex created by the outward effusion jet at the leading edge of the dilution hole, shown in Fig. 7(*b*), caused significantly more downward motion toward the leading edge of the dilution hole. For the inward case, shown in Fig. 7(*c*), the effusion jet at the leading edge of the dilution hole lifted off the surface and was entrained directly into the dilution jet. Compared to the closed and outward cases, the effusion jet at the leading edge of the dilution hole for the inward case significantly reduced the downward motion at the leading edge of the dilution hole due to the upward momentum of the effusion jet.

Figures 8(*a*)–8(*c*) show close up turbulence level contours with velocity vectors downstream of the dilution hole. Note that the field of view downstream of the dilution hole is twice the size of the field of view upstream of the dilution hole, shown in Figs. 7(*a*)–7(*c*), to illustrate the effects of the effusion jets that extended farther downstream. As was previously mentioned, the flowfield

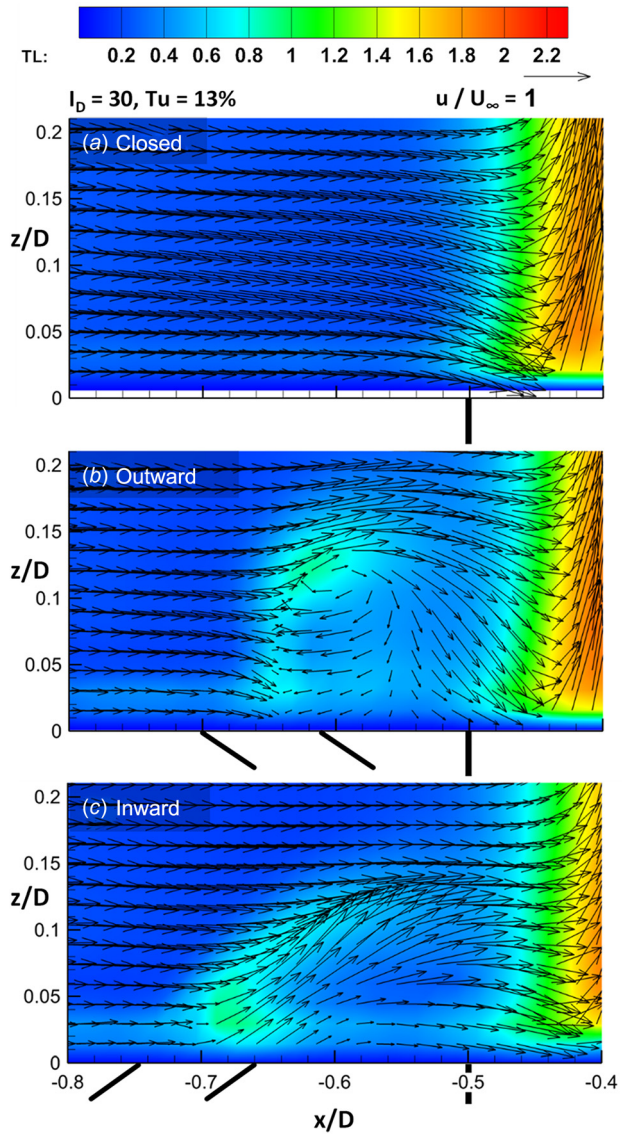

Fig. 7 Contours of the turbulence level and time-averaged velocity vectors in the centerline plane, upstream of the dilution jet for the (*a*) closed, (*b*) outward, and (*c*) inward geometries at $I_D = 30$, Tu = 13%

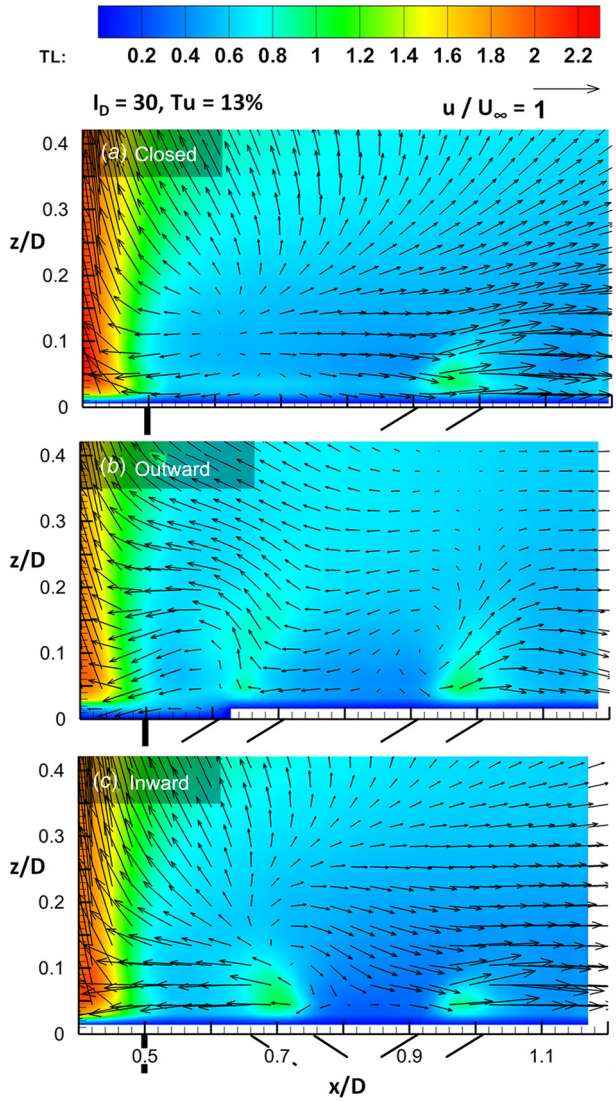

Fig. 8 Contours of the turbulence level and time-averaged velocity vectors in the centerline plane, downstream of the dilution jet for the (*a*) closed, (*b*) outward, and (*c*) inward geometries at $I_D = 30$, Tu = 13%. Note that the field of view is from $x/D = 0.4$–1.2.

downstream of the dilution hole was notably different for the outward effusion cooling pattern relative to the closed and inward cases. The outward case (Fig. 8(*b*)) was most unique compared to the other two geometries downstream of the dilution hole. The reason that the closed and inward cases were more similar downstream of the dilution hole compared to the outward case was because the inward effusion jet injected directly into the dilution jet and did not impact the downstream flow as much as the outward effusion jet did.

Compared to the flowfields upstream of the dilution hole (Figs. 7(*a*)–7(*c*)), the magnitudes of the velocities downstream (Figs. 8(*a*)–8(*c*)) were lower in the wake of the dilution jet. Note that the scale of the velocity vectors in Figs. 8(*a*)–8(*c*) are magnified compared to the vectors shown in Figs. 7(*a*)–7(*c*). In addition, compared to the effusion jets upstream of the dilution hole, the region of high turbulence downstream of the dilution jets resulted in the effusion jets quickly mixing with the mainstream. However, the turbulence levels in the cores of the downstream effusion jets were comparable to the turbulence levels in the upstream effusion jet cores.

As mentioned before, there was a clear stagnation region from which the flow emanates at $x/D = 0.6$ for the closed case, shown in Fig. 8(*a*). A similar stagnation region occurred in the inward case (Fig. 8(*c*)) at $x/D = 0.75$; however, due to the shear from inward blowing effusion jet at the trailing edge of the dilution hole, a weak vortex developed around the stagnation region. In comparing the inward case to the closed case, there was strong reverse flow between $x/D = 0.5$–0.7, resulting from the added momentum of the inward blowing effusion jet that was entrained into the dilution jet. Additionally, in the region between the two effusion holes downstream of the dilution hole ($0.75 < x/D < 0.95$), there was downward motion in the inward case, which was induced by the weak vortex.

Compared to the closed and inward cases (Figs. 8(*a*) and 8(*c*)), the downstream flowfield of the outward case (Fig. 8(*b*)) was significantly different due to the interactions of the two downstream effusion jets. As mentioned before, the effusion jet at the trailing edge of the dilution hole for the outward geometry was entrained by the strong dilution jet, which resulted in an upward trajectory of the effusion jet. Due to the trajectory, the outward blowing effusion jet entrained flow from farther downstream toward the dilution jet and the shear between the entrained flow and the row 15 effusion jet resulted in the formation of a vortex just upstream

of the row 15 effusion jet at $x/D = 0.9$. There was also downward motion at the trailing of the dilution hole in the outward case. However, compared to the flow upstream of the dilution hole, shown in Figs. 7(*a*)–7(*c*), the magnitude of downward motion at the trailing edge of the dilution hole was much less.

Effects of Momentum Flux Ratio. Flowfield measurements were made for each effusion hole pattern for three momentum flux ratios of the dilution jet, $I_D = 30$, 20, and 11, at an approaching freestream turbulence intensity of Tu = 13%. As mentioned in the "Experimental Methods" section, the dilution holes and effusion holes were supplied by the same plenum, which meant that as the momentum flux ratio of the dilution jets decreased, so did the momentum flux ratio of the effusion jets. Figures 9(*a*)–9(*i*) show the turbulence level contours with time-averaged streamlines for each geometry at Tu = 13% and each momentum flux ratio. For all cases, decreasing the momentum flux ratio resulted in lower turbulence levels in the shear layer of the dilution jet due to a decreased velocity gradient between the dilution jet and freestream. Additionally, at the lowest momentum flux ratio of the dilution jet, $I_D = 11$, there was a noticeable bend in the dilution jet for all geometries. Similar to the dilution jets for each geometry, the turbulence levels of the effusion jets decreased with decreasing momentum flux ratio of the dilution jet, which would be expected since the effusion momentum flux ratio was also decreasing. Upstream of the dilution hole, decreasing the momentum flux ratio did not significantly impact the streamlines for any of the geometries. However, the vortex that formed at the leading edge of the dilution hole for the outward cases weakened with decreasing momentum flux ratio, as shown in Figs. 9(*d*)–9(*f*).

Downstream of the dilution jet there were noticeable differences that occurred in the near-wall region for the closed and inward cases between the highest and lowest momentum flux ratios, shown in Figs. 9(*a*)–9(*c*) and 9(*g*)–9(*i*). For the closed case,

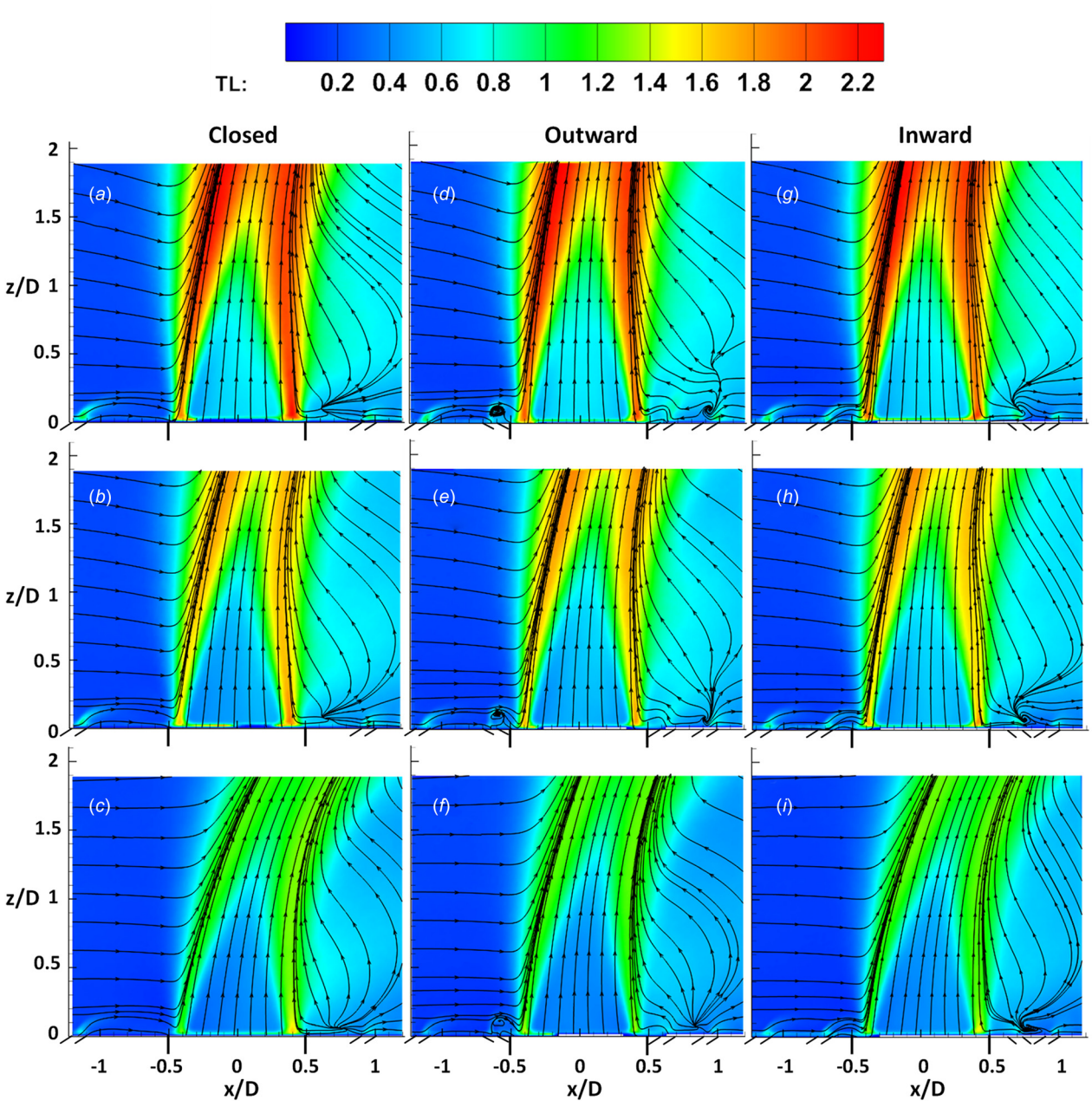

Fig. 9 Contours of turbulence level with time-averaged streamlines at Tu = 13% for (*a*) closed, $I_D = 30$, (*b*) closed, $I_D = 20$, (*c*) closed, $I_D = 11$, (*d*) outward, $I_D = 30$, (*e*) outward, $I_D = 20$, (*f*) outward, $I_D = 11$, (*g*) inward, $I_D = 30$, (*h*) inward, $I_D = 20$, and (*i*) inward, $I_D = 11$

Figs. 9(*a*) and 9(*b*) show that for $I_D = 30$ and 20, respectively, decreasing the momentum flux ratio had negligible effect on the near-wall flowfield pattern. However, in Fig. 9(*c*), which shows the closed case at $I_D = 11$, the stagnation region moved closer to the surface, indicating that flow closest to the wall was entrained into the dilution jet, as compared to the higher momentum flux ratio cases. The increased entrainment of near-wall flow from the $I_D = 11$ case was the result of the dilution jet bending closer to the surface. In correspondence with the current study, Fric and Roshko [2] found that for a jet in crossflow the wake structure downstream of the jet was dependent on how much the jet was bent toward the surface. Similar to the closed cases, there were no significant differences in the near-wall flowfield downstream of the dilution hole for the inward cases at $I_D = 30$ and 20, shown in Figs. 9(*g*) and 9(*h*). Also similar to the closed cases, the stagnation region downstream of the dilution jet for the inward, $I_D = 11$ case moved closer to the surface in comparison to the $I_D = 30$ and 20 cases.

Unlike the closed and inward cases, shown in Figs. 9(*a*)–9(*c*) and 9(*g*)–9(*i*), there were significant differences in the near-wall flowfield downstream of the dilution jet for the outward cases at each momentum flux ratio, shown in Figs. 9(*d*)–9(*f*). As the momentum flux ratio decreased from $I_D = 30$ (Fig. 9(*d*)) to $I_D = 20$ (Fig. 9(*e*)), which also decreased the momentum flux ratio of the effusion jets, the vortex at $x/D = 0.9$, weakened due to the decreased velocity gradient from the row 15 effusion jet. As the momentum flux ratio of the dilution jet decreased to $I_D = 11$, the combined effects of increased entrainment into the dilution jet and the weaker effusion jets, which resulted in less entrainment of downstream flow and decreased velocity gradient from the row 15 effusion jet, caused the vortex to completely disappear. Similar to the closed and inward cases, there was also more upward motion resulting from the entrainment into the dilution jet for the outward case at $I_D = 11$ compared to the higher momentum flux ratio cases. In comparing all of the geometries to each other, the flowfields downstream of the dilution hole for each geometry were more similar to each other at $I_D = 11$ compared to $I_D = 30$ and 20. The similarity of the flowfields at the lowest momentum flux ratio of the dilution jet for the three geometries is expected because the impact of the effusion holes decreased and the impact of the dilution jet increased with decreasing momentum flux ratio.

To compare the flowfields to the cooling effectiveness, Fig. 10 shows the centerline overall effectiveness of each geometry at $I_D = 30$, which was presented in a companion paper [1]. Figure 10 also shows the centerline effectiveness for each geometry at $I_D = 11$. The peaks in effectiveness represent the locations of the effusion hole outlets. Near the dilution hole the outward and inward cases had additional peaks in effectiveness, compared to the closed case, due to the additional effusion holes. The increased effectiveness levels of the outward and inward effusion holes also extended upstream and downstream of each respective effusion hole, as compared to the closed cases. However, the flowfields showed significant jet lift-off and the surface temperature measurements showed no coolant trails attaching to the surface, which indicated that the additional cooling was from in-hole convection. Because the outward effusion holes extended closer to the dilution hole than the inward effusion holes, the outward case was more effective at cooling the surface closer to the leading and trailing edges of the dilution hole through in-hole convection. The outward case also showed slightly better cooling effectiveness downstream of the row 15 effusion hole compared to the other geometries.

As shown in Fig. 10, the effect of the momentum flux ratio of the dilution jet on overall effectiveness was relatively small upstream of the dilution hole, which was consistent with the relatively small changes in the flowfields upstream of the dilution hole with varying momentum flux ratio. However, downstream of the dilution hole, from $x/D = 0.5$–1, there was a significant reduction in effectiveness at $I_D = 11$ compared to $I_D = 30$ for each geometry. This reduction in effectiveness was consistent with previous work by Vakil and Thole [12] and Scrittore et al. [14]. Vakil and Thole found that the film layer behind the dilution jet was thinner compared to layer upstream. Scrittore et al. found that the thinner downstream film layer was caused by entrainment into the dilution jet. Scrittore et al. also found that this reduction in effectiveness was minimized at higher momentum flux ratios of the effusion jets due to the presence of more coolant. In correspondence with the previous studies, there was a greater difference in the effectiveness between the $I_D = 30$ and 11 cases downstream of the dilution hole compared to upstream of the dilution hole due the increased entrainment of the coolant layer into the dilution jet. Additionally, the effectiveness was decreased at lower momentum flux ratios of the dilution jets because there was also less coolant in the film layer due to the corresponding lower momentum flux ratio of the effusion jets.

Also shown in Fig. 10, the centerline effectiveness for each case was the same after $x/D = 1$ for $I_D = 11$, which corresponds to the similarity in downstream flow fields for each case at $I_D = 11$ shown in Figs. 9(*c*),9(*f*), and 9(*i*). In addition, the flowfields of the current study correspond with the companion study [1], which found no significant change in effectiveness between the $I_D = 30$ and 20 cases for the closed and inward geometries and a small decrease in effectiveness between the $I_D = 30$ and 20 cases for the outward geometry.

Effects of Approaching Freestream Turbulence. In addition to evaluating each geometry at Tu = 13%, flowfields were also measured at Tu = 0.5% for $I_D = 30$ to evaluate the effects of approaching freestream turbulence. Figures 11(*a*)–11(*f*) show contours of each geometry, upstream of the dilution jet at Tu = 0.5% and Tu = 13%. Note the scale change on the contours, which was done to illustrate the approaching turbulence levels. Also, note that only the upstream flowfields are shown given that the downstream flowfields were dominated by the turbulence generated by the dilution jet with relatively no effect of the approaching freestream turbulence. For the closed, outward, and inward cases at Tu = 0.5%, shown in Figs. 11(*a*)–11(*c*), respectively, the turbulence levels in the freestream were lower than in the high approaching freestream turbulence cases at Tu = 13%, shown in Figs. 11(*d*)–11(*f*), respectively. The overall streamlines for each case indicated no real effect resulting from freestream turbulence intensity. For the closed and inward geometries, flowfields and turbulence levels did not significantly change near the wall due to freestream turbulence. However, for the outward geometry, there were higher turbulence levels near the leading edge of the dilution

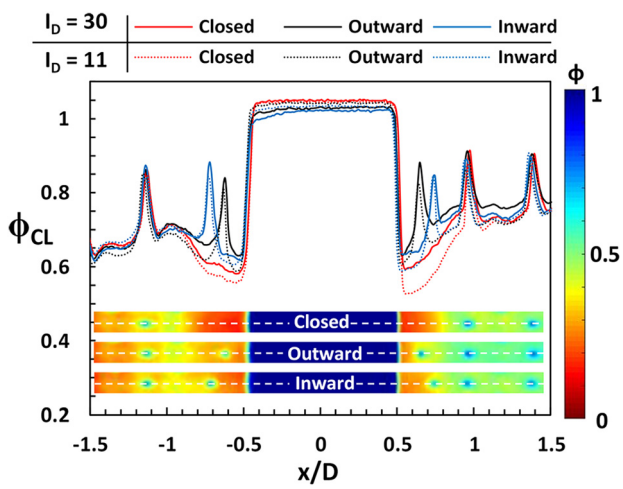

Fig. 10 Centerline overall effectiveness for each effusion hole geometry near the dilution hole for $I_D = 30$ and 11 at Tu = 13%. Note the contours shown are from the $I_D = 30$ case.

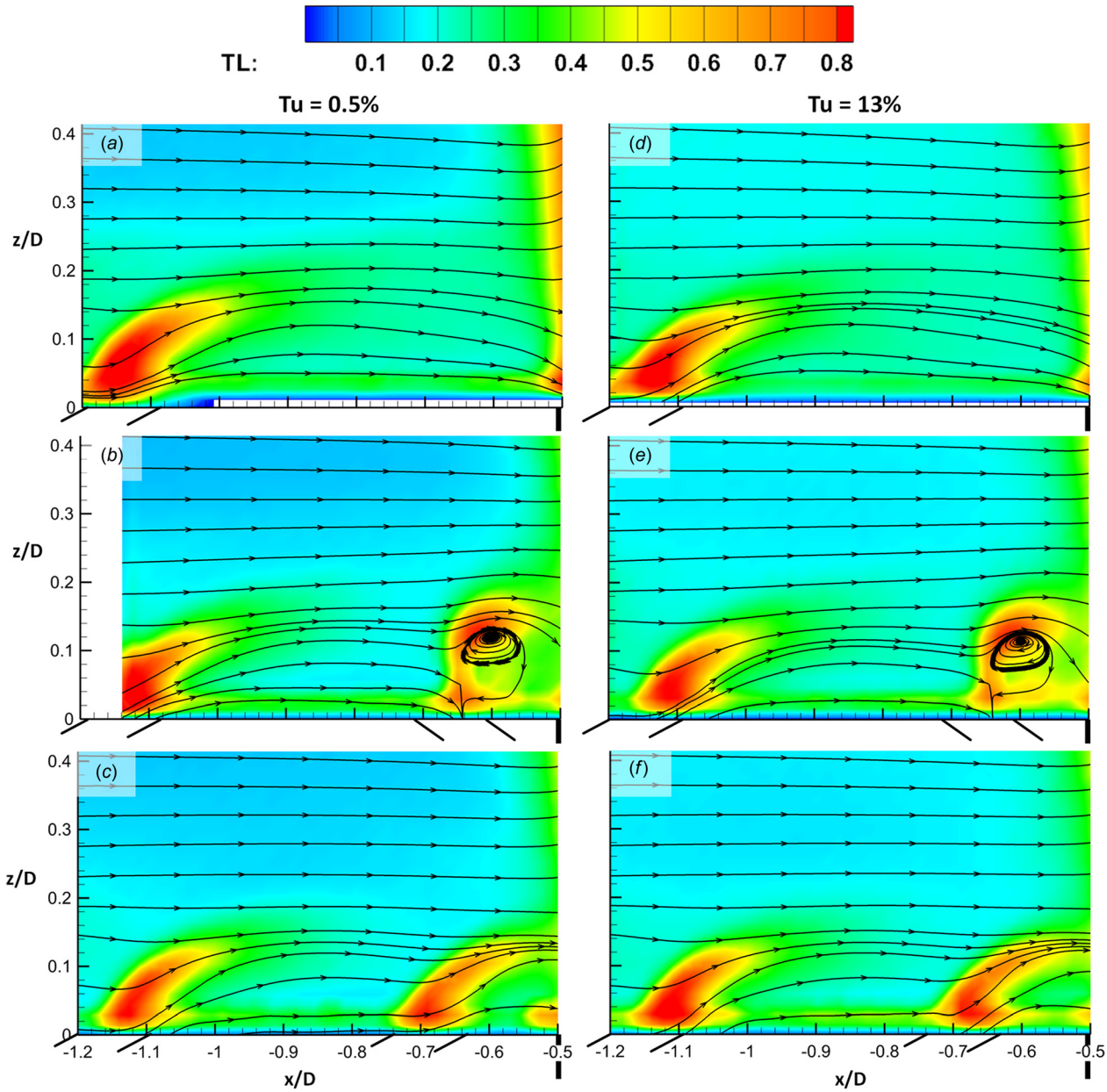

Fig. 11 Contours of turbulence level with time-averaged streamlines for (*a*) closed, Tu = 0.5%, (*b*) outward, Tu = 0.5%, (*c*) inward, Tu = 0.5%, (*d*) closed, Tu = 13%, (*e*) outward, Tu = 13%, and (*f*) inward, Tu = 13% at $I_D = 30$ upstream of the dilution jet. Note the scale of the turbulence level contours is from 0 to 0.8.

hole for the Tu = 13% case (Fig. 11(*e*)) compared to Tu = 0.5% case (Fig. 11(*b*)).

Conclusions

The flowfields for three effusion cooling hole patterns of a double-walled combustor liner were evaluated with particular attention to the near-wall flow at the leading and trailing edges of the dilution holes. The different effusion patterns located radially surrounding the dilution hole that were evaluated included: no effusion cooling holes (closed), effusion holes blowing radially outward from the dilution hole (outward), and effusion holes blowing radially inward from the dilution hole (inward). The flowfields were measured over a range of momentum flux ratios of the dilution jets and approaching freestream turbulence intensities.

The outward effusion hole pattern was found to produce a unique flowfield that significantly differed from that of the closed and inward cases. Coherent vortices formed both upstream and downstream of the dilution hole as a result of the outward effusion jets. In contrast, the inward effusion jets were entrained directly into the dilution jet and did not significantly alter the flowfield compared to the closed case. In addition, decreasing the momentum flux ratio from $I_D = 30$–20 had a noticeable impact on the downstream flowfield for the outward effusion hole pattern, but did not have an effect on the closed and inward effusion hole patterns. At the lowest momentum flux ratios for all geometries, there was a noticeable bend in the dilution jet, which resulted in entrainment of fluid from closer to the surface downstream of the dilution hole, relative to the higher momentum flux ratio cases. The flowfield measurements indicated no significant effect near the dilution hole from varying the approaching freestream turbulence intensity for each of the three effusion hole pattern.

A key finding from this research was that at the leading edge of the dilution hole, each effusion hole pattern resulted in some degree of entrainment into the dilution hole. However, for the

outward case, there was a formation of a vortex at the leading edge of the dilution hole, which increased the downward velocity toward the dilution hole compared to the closed and inward cases. Although a companion study [1] found that the outward holes resulted in better surface cooling closer to the leading edge of the dilution hole, as compared to the closed and inward cases, the increased downward velocity due to the vortex created by the outward effusion jets could lead to ingestion of freestream fluid into the dilution hole. Conversely, the upward momentum of the inward blowing effusion jet counteracted some of the downward velocity at the leading edge of the dilution hole compared to the closed and outward cases.

Acknowledgment

The authors would like to thank Pratt & Whitney for their financial and technical assistance throughout this study.

Nomenclature

b = turbulence grid bar diameter
d = effusion hole diameter
D = dilution hole diameter
DR = density ratio of coolant to mainstream, ρ_c/ρ_∞
H = distance between impingement and effusion plates
I = momentum flux ratio, $\rho_c U_c^2/\rho_\infty U_\infty^2$
l = characteristic length
L = length of effusion hole
M = blowing ratio, $\rho_c U_c/\rho_\infty U_\infty$
$\mathrm{Re_{in}}$ = inlet Reynolds number, $U_\infty l/\nu$
$S_{p,d}$ = pitchwise spacing of effusion holes
$S_{s,d}$ = spanwise spacing of effusion holes
t = thickness of effusion and impingement plates
T = temperature
TL = turbulence level, $\sqrt{(u'^2 + w'^2)/2}/U_\infty$
Tu = freestream turbulence intensity, $\sqrt{(u'^2_\infty + w'^2_\infty)/2}/U_\infty$
U_∞ = mainstream velocity
u, w = x- and z-velocities
VR = velocity ratio, U_c/U_∞
x, y, z = position measured from origin at the center of the dilution hole

Greek Symbols

α = hole injection angle
ν = kinematic viscosity
ϕ = overall effectiveness $(T_\infty - T_w)/(T_\infty - T_c)$

Subscripts

c = coolant
CL = centerline
D = dilution hole
eff = effusion hole
eff,in = effusion hole based on inlet conditions
w = wall
∞ = mainstream

Superscript

$'$ = fluctuating/rms value

References

[1] Shrager, A. C., Thole, K. A., and Mongillo, D., 2018, "Effects of Effusion Cooling Pattern Near the Dilution Hole for a Double-Walled Combustor Liner—Part 1: Overall Effectiveness Measurements," ASME Paper No. GT2018-77288.
[2] Fric, T. F., and Roshko, A., 1994, "Vortical Structure in the Wake of a Transverse Jet," J. Fluid Mech., **279**(1), pp. 1–47.
[3] Kelso, R. M., Lim, T. T., and Perry, A. E., 1996, "An Experimental Study of Round Jets in Cross-Flow," J. Fluid Mech., **306**(1), p. 111.
[4] Andreopoulos, J., 1982, "Measurements in a Jet-Pipe Flow Issuing Perpendicularly Into a Cross Stream," ASME J. Fluids Eng., **104**(4), p. 493.
[5] Peterson, S., and Plesniak, M., 2002, "Short-Hole Jet-in-Crossflow Velocity Field and Its Relationship to Film-Cooling Performance," Exp. Fluids, **33**(6), pp. 889–898.
[6] Holloway, D. S., and Walters, D. K., 2005, "Computational Study of Jet-in-Crossflow and Film Cooling Using a New Unsteady-Based Turbulence Model," ASME Paper No. GT2005-68155.
[7] Sykes, R. I., Lewellen, W. S., and Parker, S. F., 1986, "On the Vorticity Dynamics of a Turbulent Jet in a Crossflow," J. Fluid Mech., **168**(1), p. 393.
[8] Scrittore, J. J., 2008, "Experimental Study of the Effect of Dilution Jets on Film Cooling Flow in a Gas Turbine Combustor," Virginia Polytechnic Institute and State University, Blacksburg, VA.
[9] Holdeman, J. D., and Walker, R. E., 1977, "Mixing of a Row of Jets With a Confined Crossflow," AIAA J., **15**(2), pp. 243–249.
[10] Scrittore, J. J., Thole, K. A., and Burd, S. W., 2007, "Investigation of Velocity Profiles for Effusion Cooling of a Combustor Liner," ASME J. Turbomach., **129**(3), pp. 518–526.
[11] Fric, T. F., Campbell, R. P., and Rettig, M. G., 1997, "Quantitative Visualization of Full-Coverage Discrete Hole Film Cooling," ASME Paper No. 97-GT-328.
[12] Vakil, S. S., and Thole, K. A., 2005, "Flow and Thermal Field Measurements in a Combustor Simulator Relevant to a Gas Turbine Aeroengine," ASME J. Eng. Gas Turbines Power, **127**(2), p. 257.
[13] Martiny, M., Schulz, A., Wittig, S., and Dilzer, M., 1997, "Influence of a Mixing-Jet on Film Cooling," ASME Paper No. 97-GT-247.
[14] Scrittore, J. J., Thole, K. A., and Burd, S. W., 2005, "Experimental Characterization of Film-Cooling Effectiveness Near Combustor Dilution Holes," ASME Paper No. GT2005-68704.
[15] Schroeder, R. P., and Thole, K. A., 2016, "Effect of High Freestream Turbulence on Flowfields of Shaped Film Cooling Holes," ASME J. Turbomach., **138**(9), pp. 1–10.
[16] LaVision, 2015, "Product Manual for DaVis 8.3.0," LaVision, Göttingen, Germany.
[17] Moffat, R. J., 1985, "Using Uncertainty Analysis in the Planning of an Experiment," ASME J. Fluids Eng., **107**(2), p. 173.
[18] Figliola, R. S., and Beasley, D. E., 2011, *Theory and Design for Mechanical Measurements*, Wiley, Hoboken, NJ.